Materials Research Bulletin 60 (2014) 5–9

Contents lists available at ScienceDirect

Materials Research Bulletin

journal homepage: www.elsevier.com/locate/matresbu

Electrochemical performance studies of MnO_2 nanoflowers recovered from spent battery

Gomaa A.M. Ali [a,b], Ling Ling Tan [c], Rajan Jose [a], Mashitah M. Yusoff [a], Kwok Feng Chong [a,*]

[a] Faculty of Industrial Sciences & Technology, Universiti Malaysia Pahang, 26300 Gambang, Kuantan,Pahang, Malaysia
[b] Chemistry Department, Faculty of Science, Al-Azhar University, Assiut 71524, Egypt
[c] Southeast Asia Disaster Prevention Research Initiative (SEADPRI-UKM), LESTARI, Universiti Kebangsaan Malaysia, 43600 UKM Bangi, Selangor, Malaysia

ARTICLE INFO

Article history:
Received 11 February 2014
Received in revised form 1 August 2014
Accepted 11 August 2014
Available online 13 August 2014

Keywords:
Electrochemical properties
Energy storage
Nanostructures
Oxides

ABSTRACT

The electrochemical performance of MnO_2 nanoflowers recovered from spent household zinc–carbon battery is studied by cyclic voltammetry, galvanostatic charge/discharge cycling and electrochemical impedance spectroscopy. MnO_2 nanoflowers are recovered from spent zinc–carbon battery by combination of solution leaching and electrowinning techniques. In an effort to utilize recovered MnO_2 nanoflowers as energy storage supercapacitor, it is crucial to understand their structure and electrochemical performance. X-ray diffraction analysis confirms the recovery of MnO_2 in birnessite phase, while electron microscopy analysis shows the MnO_2 is recovered as 3D nanostructure with nanoflower morphology. The recovered MnO_2 nanoflowers exhibit high specific capacitance (294 $F g^{-1}$ at 10 $mV s^{-1}$; 208.5 $F g^{-1}$ at 0.1 $A g^{-1}$) in 1 M Na_2SO_4 electrolyte, with stable electrochemical cycling. Electrochemical data analysis reveal the great potential of MnO_2 nanoflowers recovered from spent zinc–carbon battery in the development of high performance energy storage supercapacitor system.

1. Introduction

Zinc–carbon battery is frequently used in electronic and electrical appliances as it is the least expensive battery among primary batteries. Fresh zinc–carbon battery consists of Zn metal as anode and MnO_2 powder as cathode. In discharged form, Zn is present as ZnO, while Mn is present as Mn_2O_3 and Mn_3O_4[1–3]. Research shows that Zn and Mn contents are 28.3% and 26.3%, respectively of the total mass in a spent zinc–carbon battery [2]. Such high Zn and Mn contents highlight the importance of battery recycling, both from economy and environment perspectives. Battery recycling can be divided into pyrometallurgical process and hydrometallurgical process. The former involves selective volatization of scrapped battery at elevated temperature followed by condensation for metal recovery. It is the most popular battery recycling process in industry due to its simplicity as battery dismantling is not required [3–6]. On the other hand, hydrometallurgical process involves dismantling, pre-treatment followed by metal ions leaching and precipitation. Hydrometallurgical process is more efficient in metal recovery and environmental friendly as its energy consumption is lower [7,8]. A comparison of these processes is reported elsewhere [9], with detail technical information about battery treatment. However, battery recycling activities are not favored all the time as the economic interests normally supersede the environmental obligations. Therefore, recycling spent battery into valuable product is expected to be a solution in this context. In this work, we study the feasibility of recovered MnO_2 from spent zinc–carbon battery in supercapacitor application.

Supercapacitor is an energy storage device that stores energy via ion adsorption (electrochemical double layer capacitor) or fast surface redox reaction (pseudocapacitor). It has attracted worldwide research interests, mainly attributed to its high power capability, fast charging time, excellent reversibility and long cycle life [10]. In terms of energy and power aspects, supercapacitor positions between battery and conventional capacitor where it is preferred when high power load is needed. Recent years, various materials have been developed for supercapacitor electrode and they can be categorized into carbon-based materials (activated carbon, carbon nanotubes, graphene, fullerene) [11–14], transition metal oxides ($RuO_2{\cdot}H_2O$, MnO_2, Co_3O_4, V_2O_5) [15–18], and conductive polymers (polyaniline, polypyrrole) [19,20]. Among these materials, transition metal oxides show superiority over the rest due to their high specific capacitance. $RuO_2{\cdot}H_2O$ is a remarkable transition metal oxide as it can contribute specific capacitance up to 1585 $F g^{-1}$ [15]. Nonetheless, its commercial

* Corresponding author. Tel.: +60 9 5492403; fax: +60 9 5492766.
E-mail address: ckfeng@ump.edu.my (K.F. Chong).

http://dx.doi.org/10.1016/j.materresbull.2014.08.008
0025-5408/

application is dampened due to its toxicity and high cost. Various efforts have been attempted to find a cheap yet environmental friendly material to replace $RuO_2{\cdot}H_2O$ as supercapacitor electrode. MnO_2 is found to be a potential candidate for this purpose due to its environmental friendly nature, low cost and high pseudocapacitance with reversible redox transition between III and IV oxidation states [21,22]. Various synthesis routes for MnO_2 have been developed, such as hydrothermal [23], thermal decomposition [24], sol–gel [25], electrodeposition [26] and microwave-assisted [27] syntheses. In addition, different morphologies such as nanowires [28], nanorods [29], nanoflowers [30] and nanoflakes [31] have been prepared as the pseudocapacitance of MnO_2 is highly influenced by its morphology. Regardless of the synthesis routes or the MnO_2 morphologies, all the reported works used manganese precursors such as $MnSO_4$, $KMnO_4$ or $Mn(CH_3COO)_2$ from the commercial chemical source. To the best of our knowledge, the preparation of MnO_2 from waste source has not been reported yet. The aim of the present work is to study the electrochemical performance of MnO_2 recovered from spent household zinc–carbon battery and to evaluate its potential as energy storage supercapacitor.

2. Experimental section

A spent Zn–C battery (EVEREADY® D cell) was dismantled and the cathode black paste was used for subsequent process. The cathode black paste was dried at 130 °C for 24 h, ground well in a mortar, and then sieved using a 200 μm mesh. The sieved powder was later washed with deionized water (solid to liquid ratio 1:10) to remove NH_4Cl electrolyte in the battery and finally dried at 105 °C for 24 h. The dried powder (20 g) was subsequently dissolved in H_2SO_4 (200 mL, 2 M), followed by addition of $H_2C_2O_4$ (14.5 g, Aldrich, 99%) as reducing agent. The leaching was continued for 5 h at 80 °C with continuous stirring according to [3,8]:

$$Mn_2O_3 + H_2SO_4 \rightarrow MnO_2 + MnSO_4 + H_2O \quad (1)$$

$$Mn_3O_4 + 2H_2SO_4 \rightarrow MnO_2 + 2MnSO_4 + 2H_2O \quad (2)$$

$$MnO_2 + H_2C_2O_4 + H_2SO_4 \rightarrow MnSO_4 + 2CO_2 + 2H_2O \quad (3)$$

The leached solution was filtered prior to electrowinning. For electrowinning, two stainless steel plates were set up as electrodes and the distance between electrodes was kept at 20 mm. The electrowinning was carried out in leached solution (50 mL) at current density of 0.15 A cm^{-2} for 1 h at room temperature. The electrowinning involves Mn(II) oxidation to Mn(III) and followed by disproportionation to Mn(II) and Mn(IV). MnO_2 was formed as dark precipitate at the bottom of the cell. The reaction mechanism can be described as follows [32]:

$$2Mn^{2+} \rightarrow 2Mn^{3+} + 2e^- \quad (4)$$

$$2Mn^{3+} + 2H_2O \rightarrow Mn^{2+} + MnO_2 + 4H^+ \quad (5)$$

The recovered MnO_2 was investigated by means of X-ray diffraction (XRD, PHILIPS PW1700, Netherlands; Cu Kα radiation, λ = 0.154 nm), Fourier transform infrared spectrometer (FTIR, JASCO 480 Plus, USA) and field emission scanning electron microscope (FESEM, JEOL JSM-7800F, USA) for structural and morphology analyses.

For electrochemical characterization, MnO_2 electrode was prepared with a final composition of 80 wt.% recovered MnO_2, 15 wt.% carbon black (Alfa Aesar) and 5 wt.% polytetrafluoroethylene (Aldrich, 60 wt.%). The mixture was casted on nickel foam (Goodfellow) and dried at 60 °C for 30 min. After drying, the coated mesh was uni-axially pressed (5 t) and the weight of the active material was determined by a microbalance. The active material mass loading of the so-obtained electrode was 9.2 mg cm^{-2}. Three-electrode electrochemical system was set up: MnO_2 electrode as working electrode, Ag/AgCl (CH Instrument) as reference electrode and Pt wire (CH Instrument) as counter electrode. The electrochemical data was collected using an electrochemical workstation (AUTOLAB PGSTAT30, Netherlands) equipped with frequency response analyzer. Cyclic voltammetry (CV) tests were performed in the potential range between 0 V and 1 V vs. Ag/AgCl with scan rates from 10 mV s^{-1} to 100 mV s^{-1}. Charge/discharge galvanostatic tests were performed at different current densities from 0.1 A g^{-1} to 5 A g^{-1}. Electrochemical impedance spectroscopy (EIS) data were collected from 500 kHz to 1 mHz, at open circuit potential with a.c. amplitude of 10 mV. Na_2SO_4 (1 M) was used as the electrolyte throughout all electrochemical measurements. For comparison, the dried cathode powder electrode was prepared and tested similarly.

3. Results and discussion

3.1. Structural and morphology characterization

In Fig. 1, XRD analysis shows that Mn_2O_3 and Mn_3O_4 are the major phases in dried cathode powder. A sharp peak observed at 11.54° for dried cathode powder could be related to the $Zn_5(OH)_8Cl_2{\cdot}H_2O$ [8]. After electrowinning, dark precipitate of MnO_2 shows broad peaks at 12.58°, 37.14°, and 66.18°, correspond to (0 0 2), (0 0 6) and (1 1 9) planes of birnessite-type MnO_2 (JCPDS No. 00-018-0802), respectively [31–34]. No other peaks related to the impurities can be found. According to Scherrer formula [35], the crystallite size of recovered MnO_2 was calculated to be 5 nm.

Fig. 2 displays the FTIR spectrum of MnO_2 in the wavenumber range of 400–4000 cm^{-1}. The strong absorption band at 530 cm^{-1} could be assigned to the Mn—O stretching mode, indicating the presence of Mn—O bond within MnO_2 structure [36]. The absorption bands at 1634 cm^{-1} and 1124 cm^{-1} correspond to the O—H bending vibrations combined with Mn atoms, while the broad absorption band at 3439 cm^{-1} corresponds to the O—H stretching vibrations of hydroxyl group. The observation of O—H vibrations in FTIR spectrum suggests the presence of absorbed water molecules within MnO_2 structure. The hydrous properties of MnO_2 could enhance the cations diffusion thereby increasing the specific capacitance of MnO_2.

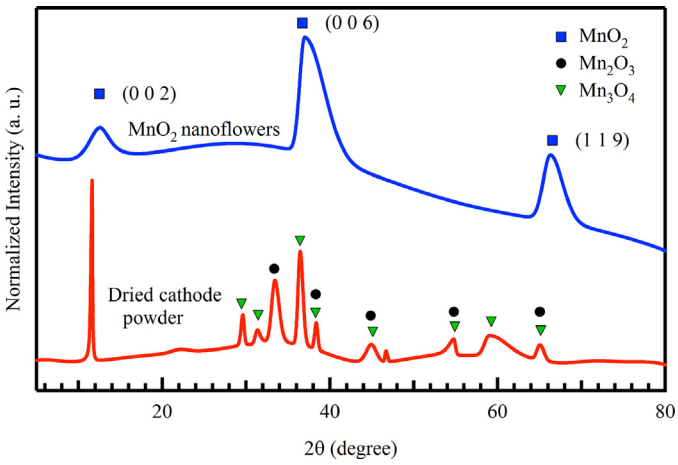

Fig. 1. XRD spectra of dried cathode powder and MnO_2 nanoflowers.

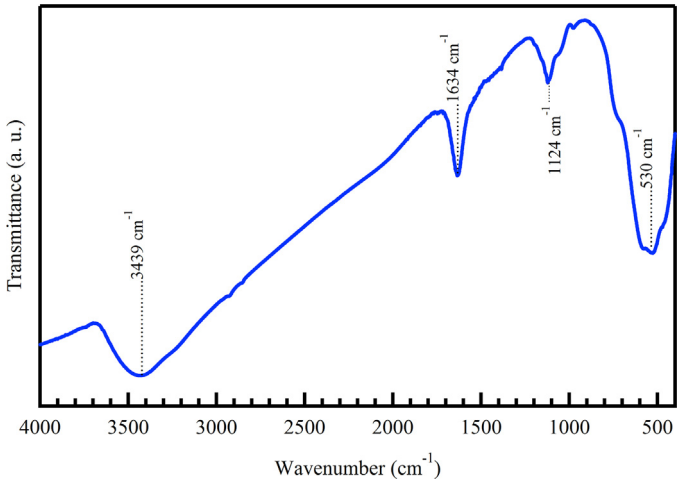

Fig. 2. FTIR spectrum of MnO_2 nanoflowers.

Representative FESEM images of dried cathode powder and recovered MnO_2 are presented in Fig. 3. It can be clearly seen that the Mn_2O_3 and Mn_3O_4 particles are randomly distributed in dried cathode powder with irregular sizes and shapes. The approximate size of these particles is ca. 100 nm, as estimated from the micrograph. The recovered MnO_2 particles appear as sheet-like structure with nanoflower morphology. Such sheet-like structure would remarkably increase the surface area, thus enhancing the specific capacitance of MnO_2.

3.2. Electrochemical studies

The charge storage properties of MnO_2 nanoflowers electrode were evaluated by CV, galvanostatic charge/discharge and EIS. In CV, MnO_2 nanoflowers electrode exhibits rectangular shape in CV (Fig. 4(a)), an indication of good charge propagation within the structure. The specific capacitance is calculated by integrating over the full CV curve for the average value. Fig. 4(b) summarizes the variation of specific capacitance of MnO_2 nanoflowers electrode as a function of scan rate. It can be clearly seen that the specific capacitance of MnO_2 nanoflowers electrode is dependent on the scan rate as the specific capacitance increases at lower scan rate. At low scan rates (10 mV s^{-1} and 25 mV s^{-1}), the cations (Na^+ and H^+) can easily diffuse and penetrate deep into the inter layer sheets of

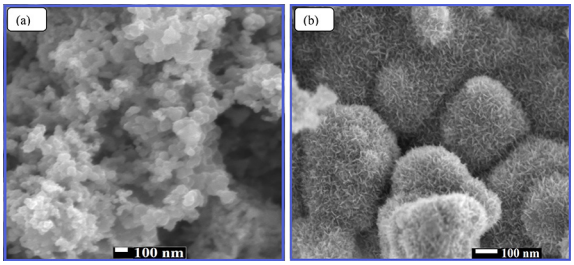

Fig. 3. Representative FESEM images of (a) dried cathode powder and (b) MnO_2 nanoflowers.

the nanoflower structure, leading to more ions adsorption and higher specific capacitance. At high scan rates (50 mV s^{-1} and 100 mV s^{-1}), the cations can only adhere to the outer surface of the nanoflower structure, contributing little to the electrochemical capacitive behavior. The charge storage mechanism for MnO_2 nanoflowers electrode is based on the intercalation/de-intercalaction of cations (Na^+ and H^+) on the nanoflower structure, which can be ascribed to the following reactions [37–39]:

$$MnO_2 + M^+ + e^- \rightarrow MnOOM\ (M^+ = Na^+ \text{ or } H^+) \quad (6)$$

$$MnO_2)_{surface} + M^+ + e^- \leftrightarrow (MnOOM)_{surface}\ (M^+ = Na^+ \text{ or } H^+) \quad (7)$$

The average specific capacitance of MnO_2 nanoflowers electrode is calculated to be 294 F g^{-1} at 10 mV s^{-1}. The obtained value is higher than of the reported value for MnO_2 films (237 F g^{-1}) [39], MnO_2 nanowires (237 F g^{-1}) [40], and MnO_2 nanoflowers (259 F g^{-1}) [30]. For control experiment, the dried cathode powder was tested (Fig. 4(a)) and it shows low capacitive behavior with 24 F g^{-1} at 10 mV s^{-1}.

The galvanostatic charge/discharge curve of MnO_2 nanoflowers electrode is displayed in Fig. 5(a). It can be clearly seen that the charge/discharge curve of MnO_2 nanoflowers electrode is linear and symmetrical with insignificant iR drop. It can be attributed to the rapid current–voltage response and good electrochemical reversibility of MnO_2 nanoflowers electrode. The specific capacitance is calculated from the slope of the discharge curve. As shown in Fig. 5(b), the specific capacitance is 208.5 F g^{-1} at current density of 0.1 A g^{-1} and the value slightly decreases to 174.2 F g^{-1} when the current density increases to 5 A g^{-1}, thereby indicating the MnO_2

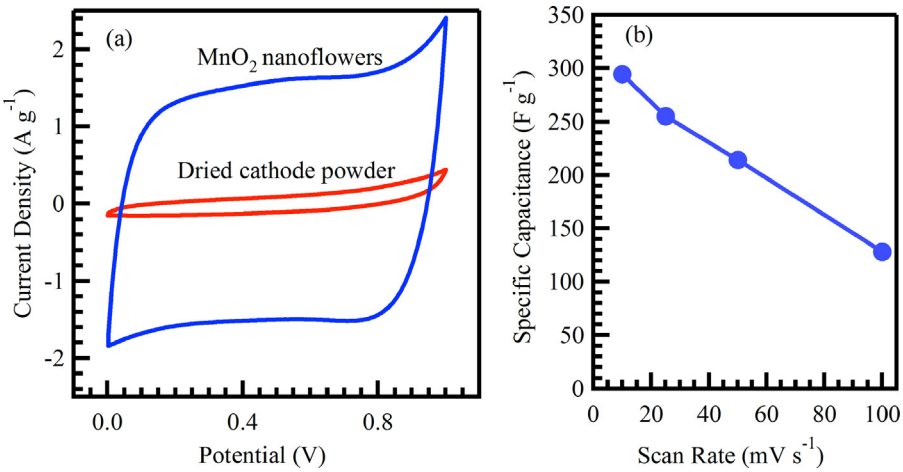

Fig. 4. (a) Cyclic voltammograms of dried cathode powder electrode and MnO_2 nanoflowers electrode at 10 mV s^{-1} in 1 M Na_2SO_4; (b) variation of specific capacitance for MnO_2 nanoflowers electrode as a function of scan rate.

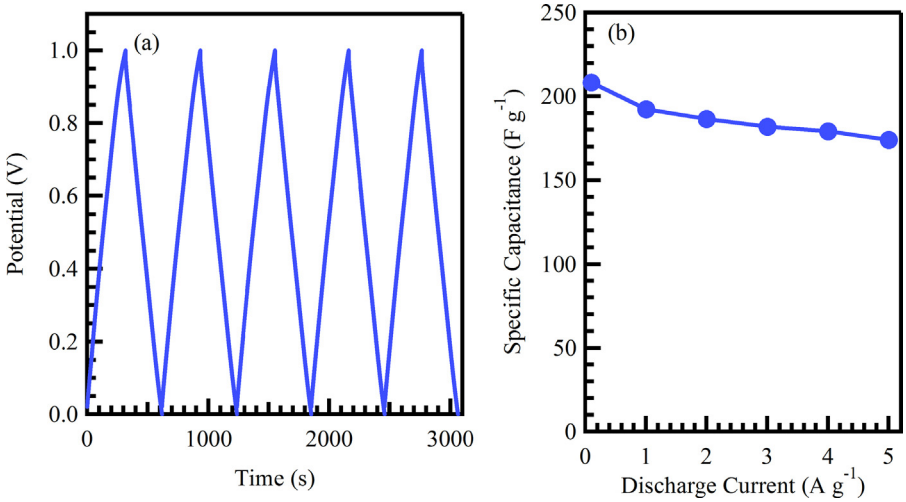

Fig. 5. (a) Galvanostatic charge–discharge curve of MnO_2 nanoflowers electrode at 0.5 A g^{-1} in 1 M Na_2SO_4; (b) variation of specific capacitance for MnO_2 nanoflowers electrode as a function of current density.

nanoflowers electrode could be charged/discharged under high current density.

The electrochemical cycling stability is a crucial factor for the supercapacitor application. Fig. 6 shows the cycling stability test for MnO_2 nanoflowers electrode at current density of 1 A g^{-1}. During the first 200 cycles, it can be noticed that the capacitance retention gradually drops to ~88% and remains constant up to 900 cycles. We attribute the capacitance drop during the initial cycling process to the stacking of nanoflowers structure that leads to lower surface area contacts with the electrolyte ions. However, such high capacitance retention up to 900 cycles suggests that the MnO_2 recovered from zinc–carbon battery is a good candidate for supercapacitor application.

The EIS data is analyzed with Nyquist plot. It shows the frequency response at the electrode/electrolyte system and is a profile of imaginary component (Z″) of the impedance against the real component (Z′). The Nyquist plot of MnO_2 nanoflowers electrode (Fig. 7) features a semicircle at high frequencies followed by a near vertical line at low frequencies. The intersection at *X*-axis represents the bulk solution resistance (R_Ω), consisting of electrolyte resistance, intrinsic resistance of substrate and contact resistance between active material and current collector. The R_Ω is estimated at ca. 2.10 Ω. The semicircle at high frequencies corresponds to the charge transfer resistance (R_{CT}) of MnO_2 nanoflowers electrode and it is estimated at ca. 2.01 Ω, lower as compared to other reported values for MnO_2 [39,41]. The transition between resistance and capacitance behaviors is observed at the frequency of about ca. 5.35 Hz (Fig. 7 inset). This suggests that most of the energy stored in MnO_2 nanoflowers electrode can be accessible at frequencies below 5.35 Hz. The near vertical line at low frequencies indicates the nearly ideal capacitive behavior of MnO_2 nanoflowers electrode. The time constant (τ) of MnO_2 nanoflowers electrode is calculated according to the equation $\tau = (2\pi f_0)^{-1}$, where f_0 is the frequency corresponds to the maximum of the imaginary component of impedance ($-Z''$) of the semicircle in Nyquist plot [42]. The value of τ obtained from Fig. 7 (inset) is calculated at 1.13 ms. This value is lower as compared with the reported value for MnO_2 (2.8 ms) [43], indicating the potential of MnO_2 recovered from spent battery in the application of fast charge/discharge supercapacitor.

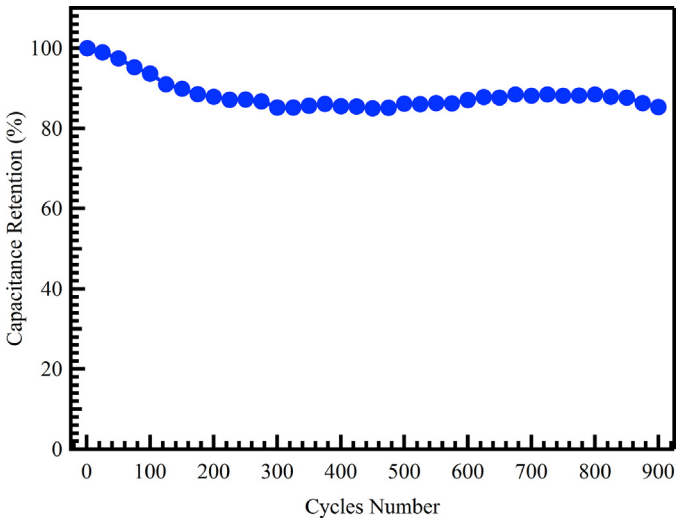

Fig. 6. Cycling stability of MnO_2 nanoflowers electrode at 1 A g^{-1} in 1 M Na_2SO_4.

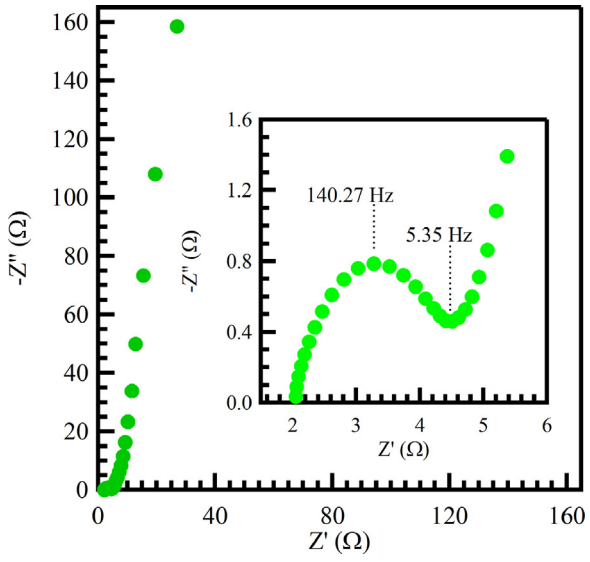

Fig. 7. Nyquist plot of MnO_2 nanoflowers electrode at open circuit potential in 1 M Na_2SO_4; inset shows magnified Nyquist plot at high frequencies region.

4. Conclusions

MnO_2 with nanoflower morphology is successfully recovered from zinc–carbon battery by combination of leaching and electrowinning techniques. CV and charge/discharge results show that the MnO_2 nanoflowers possess good capacitive behavior ($294\ F\ g^{-1}$ at $10\ mV\ s^{-1}$; $208.5\ F\ g^{-1}$ at $0.1\ A\ g^{-1}$) with stable cycling up to 900 cycles. In addition, EIS analysis suggests that the MnO_2 nanoflowers could be potential candidate for fast charge/discharge supercapacitor with low charge transfer resistance and low time constant. The current work reveals the great potential of MnO_2 recovered from spent zinc–carbon battery in the development of high performance energy storage supercapacitor system.

Acknowledgements

KF Chong and co-workers would like to acknowledge the funding from the Ministry of Education Malaysia in the form of MTUN-COE grant RDU121212 and RDU121213 and Ministry of Science, Technology and Innovation in the form of eScienceFund RDU140501.

References

[1] I.D. Michelis, F. Ferella, E. Karakaya, F. Beolchini, F. Vegliò, Recovery of zinc and manganese from alkaline and zinc–carbon spent batteries, J. Power Sources 172 (2007) 975.
[2] E. Sayilgan, T. Kukrer, G. Civelekoglu, F. Ferella, A. Akcil, F. Veglio, M. Kitis, A review of technologies for the recovery of metals from spent alkaline and zinc–carbon batteries, Hydrometallurgy 97 (2009) 158;1;.
[3] R. Rácz, P. Ilea, Electrolytic recovery of Mn3O4 and Zn from sulphuric acid leach liquors of spent zinc–carbon–MnO_2 battery powder, Hydrometallurgy 139 (2013) 116.
[4] Y. Li, G. Xi, The dissolution mechanism of cathodic active materials of spent Zn–Mn batteries in HCl, J. Hazard. Mater. 127 (2005) 244.
[5] J. Nan, D. Han, M. Cui, M. Yang, L. Pan, Recycling spent zinc manganese dioxide batteries through synthesizing Zn–Mn ferrite magnetic materials, J. Hazard. Mater. 133 (2006) 257.
[6] A.L. Salgado, A.M.O. Veloso, D.D. Pereira, G.S. Gontijo, A. Salum, M.B. Mansur, Recovery of zinc and manganese from spent alkaline batteries by liquid–liquid extraction with Cyanex 272, J. Power Sources 115 (2003) 367.
[7] M.B.J.G. Freitas, V.C. Pegoretti, M.K. Pietre, Recycling manganese from spent Zn–MnO_2 primary batteries, J. Power Sources 164 (2007) 947.
[8] F. Ferella, I.D. Michelis, F. Veglio, Process for the recycling of alkaline and zinc–carbon spent batteries, J. Power Sources 183 (2008) 805.
[9] A.M. Bernardes, D.C.R. Espinosa, J.A.S. Tenorio, Recycling of batteries: a review of current processes and technologies, J. Power Sources 130 (2004) 291.
[10] Y. Zhang, H. Feng, X. Wu, L. Wang, A. Zhang, T. Xia, H. Dong, X. Li, L. Zhang, Progress of electrochemical capacitor electrodematerials: a review, Int. J. Hydrogen Energy 34 (2009) 4889.
[11] D. Qu, H. Shi, Studies of activated carbons used in double-layer capacitors, J. Power Sources 74 (1998) 99.
[12] G. Lota, K. Fic, E. Frackowiak, Carbon nanotubes and their composites in electrochemical applications, Energy Environ. Sci. 4 (2011) 1592.
[13] Y. Zhu, S. Murali, M.D. Stoller, K.J. Ganesh, W. Cai, P.J. Ferreira, A. Pirkle, R.M. Wallace, K.A. Cychosz, M. Thommes, D. Su, E.A. Stach, R.S. Ruoff, Carbon-based supercapacitors produced by activation of graphene, Science 332 (2011) 1537.
[14] K. Okajima, A. Ikeda, K. Kamoshita, M. Sudoh, High rate performance of highly dispersed C_{60} on activated carbon capacitor, Electrochim. Acta 51 (2005) 972.
[15] A. Ponrouch, S. Garbarino, E. Bertin, D. Guay, Ultra high capacitance values of Pt@RuO_2 core–shell nanotubular electrodes for microsupercapacitor applications, J. Power Sources 221 (2013) 228.
[16] W. Wei, X. Cui, W. Chen, D.G. Ivey, Manganese oxide-based materials as electrochemical supercapacitor electrodes, Chem. Soc. Rev. 40 (2011) 1697.
[17] S.G. Kandalkar, H.-M. Lee, H. Chae, C.-K. Kim, Structural, morphological, and electrical characteristics of the electrodeposited cobalt oxide electrode for supercapacitor applications, Mater. Res. Bull. 46 (2011) 48.
[18] G. Wee, H.Z. Soh, Y.L. Cheah, S.G. Mhaisalkar, M. Srinivasan, Synthesis and electrochemical properties of electrospun V_2O_5 nanofibers as supercapacitor electrodes, J. Mater. Chem. 20 (2010) 6720.
[19] H. Xie, Y. Zhu, Y. Wu, Z. Wu, E. Liu, The effect of hydroquinone as an electrolyte additive on electrochemical performance of the polyaniline supercapacitor, Mater. Res. Bull. 50 (2014) 303.
[20] A. Sumboja, X. Wang, J. Yan, P.S. Lee, Nanoarchitectured current collector for high rate capability of polyaniline based supercapacitor electrode, Electrochim. Acta 65 (2012) 190.
[21] S.-C. Pang, M.A. Anderson, T.W. Chapman, J. Electrochem. Soc. 147 (2000) 444.
[22] M. Toupin, T. Brousse, D. Bélanger, Charge storage mechanism of MnO_2 electrode used in aqueous electrochemical capacitor, Chem. Mater. 16 (2004) 3184.
[23] X. Duan, J. Yang, H. Gao, J. Ma, L. Jiao, W. Zheng, Controllable hydrothermal synthesis of manganese dioxide nanostructures: shape evolution, growth mechanism and electrochemical properties, CrystEngComm 14 (2012) 4196.
[24] S.H. Kim, S.J. Kim, S.M. Oh, Preparation of layered MnO_2 via thermal decomposition of $KMnO_4$ and its electrochemical characterizations, Chem. Mater. 11 (1999) 557.
[25] A.L. Tiano, C. Koenigsmann, A.C. Santulli, S.S. Wong, Solution-based synthetic strategies for one-dimensional metal-containing nanostructures, Chem. Commun. 46 (2010) 8093.
[26] M. Fukuda, C. Lida, M. Nakayama, One-step through mask electrodeposition of a porous structure composed of manganese oxide nanosheets with electrocatalytic activity for oxygen reduction, Mater. Res. Bull. 44 (2009) 1323.
[27] B. Ming, J. Li, F. Kang, G. Pang, Y. Zhang, L. Chen, J. Xu, X. Wang, Microwave-hydrothermal synthesis of birnessite-type MnO_2 nanospheres as supercapacitor electrode, J. Power Sources 198 (2012) 428.
[28] H. Jiang, T. Zhao, J. Ma, C. Yan, C. Li, Ultrafine manganese dioxide nanowire network for high-performance supercapacitors, Chem. Commun. 47 (2011) 1264.
[29] D. Su, H.-J. Ahn, G. Wang, Hydrothermal synthesis of α-MnO_2 and β-MnO_2 nanorods as high capacity cathode materials for sodium ion batteries, J. Mater. Chem. A 1 (2013) 4845.
[30] Y. Yang, C. Huang, Effect of synthetical conditions, morphology, and crystallographic structure of MnO_2 on its electrochemical behavior, J. Solid State Electrochem. 14 (2010) 1293.
[31] H. Jiang, T. Sun, C. Li, J. Ma, Hierarchical porous nanostructures assembled from ultrathin MnO_2 nanoflakes with enhanced supercapacitive performances, J. Mater. Chem. 22 (2012) 2751.
[32] C.C.B.M. de Souza, J.A.S. Tenório, Simultaneous recovery of zinc and manganese dioxide from household alkaline batteries through hydrometallurgical processing, J. Power Sources 136 (2004) 191.
[33] A.K. Thapa, B. Pandit, R. Thapa, T. Luitel, H.S. Paudel, G. Sumanasekera, M.K. Sunkara, N. Gunawardhana, T. Ishihara, M. Yoshio, Synthesis of mesoporous birnessite-MnO_2 composite as a cathode electrode for lithium battery, Electrochim. Acta 116 (2014) 188.
[34] P. Yu, X. Zhang, Y. Chen, Y. Ma, Z. Qi, Preparation and pseudo-capacitance of birnessite-type MnO_2 nanostructures via microwave-assisted emulsion method, Mater. Chem. Phys. 118 (2009) 303.
[35] A. Patterson, The Scherrer formula for X-ray particle size determination, Phys. Rev. 56 (1939) 978.
[36] G.S. Gund, D.P. Dubal, B.H. Patil, S.S. Shinde, C.D. Lokhande, Enhanced activity of chemically synthesized hybrid grapheme oxide/Mn_3O_4 composite for high performance supercapacitors, Electrochim. Acta 92 (2013) 205.
[37] J. Ni, W. Lu, L. Zhang, B. Yue, X.Y. Shang. Lv, Low-temperature synthesis of monodisperse 3D manganese oxide nanoflowers and their pseudocapacitance properties, J. Phys. Chem. C 113 (2009) 54.
[38] R.B. Rakhi, D. Cha, W. Chen, H.N. Alshareef, Electrochemical energy storage devices using electrodes incorporating carbon nanocoils and metal oxides nanoparticles, J. Phys. Chem. C 115 (2011) 14392.
[39] D.P. Dubal, D.S. Dhawale, T.P. Gujar, C.D. Lokhande, Effect of different modes of electrodeposition on supercapacitive properties of MnO_2 thin films, Appl. Surf. Sci. 257 (2011) 3378.
[40] T. Yousefi, A.N. Golikand, M.H. Mashhadizadeh, M. Aghazadeh, Template-free synthesis of MnO_0 nanowires with secondary flower like structure: characterization and supercapacitor behavior studies, Curr. Appl. Phys. 12 (2012) 193.
[41] D.P. Dubal, C.D. Lokhande, Significant improvement in the electrochemical performances of nano–nest like amorphous MnO_2 electrodes due to Fe doping, Ceram. Int. 39 (2013) 415.
[42] Y.-K. Zhou, B.-L. He, W.-J. Zhou, J. Huang, X.-H. Li, B. Wu, H.-L. Li, Electrochemical capacitance of well-coated single-walled carbon nanotube with polyaniline composites, Electrochim. Acta 49 (2004) 257.
[43] C. Yuan, B. Gao, L. Su, X. Zhang, Interface synthesis of mesoporous MnO_2 and its electrochemical capacitive behaviors, J. Colloid Interface Sci. 322 (2008) 545.